Hindawi Publishing Corporation
International Journal of Photoenergy
Volume 2015, Article ID 605690, 8 pages
http://dx.doi.org/10.1155/2015/605690

Research Article

TiO_2/Halloysite Composites Codoped with Carbon and Nitrogen from Melamine and Their Enhanced Solar-Light-Driven Photocatalytic Performance

Pengcheng Yao,[1] Shuhui Zhong,[2] and Zhurui Shen[1]

[1]*Key Laboratory for Advanced Ceramics and Machining Technology of Ministry of Education, Tianjin University & School of Material Science and Engineering, Tianjin University, Tianjin 300072, China*
[2]*School of Science, Tianjin University, Tianjin 300072, China*

Correspondence should be addressed to Shuhui Zhong; zhshuhui@tju.edu.cn and Zhurui Shen; shenzhurui@tju.edu.cn

Received 20 September 2015; Revised 26 October 2015; Accepted 28 October 2015

Academic Editor: Wanjun Wang

Copyright © 2015 Pengcheng Yao et al. This is an open access article distributed under the Creative Commons Attribution License, which permits unrestricted use, distribution, and reproduction in any medium, provided the original work is properly cited.

Carbon (C) and nitrogen (N) codoped anatase TiO_2/amorphous halloysite nanotubes (C+N-TiO_2/HNTs) were fabricated using melamine as C and N source. The samples prepared by different weight ratios of melamine and TiO_2 were investigated by X-ray diffraction (XRD) and UV-vis diffuse reflectance spectrometer. It is shown that the doping amounts of C and N could influence the photocatalytic performance of as-prepared composites. When the weight ratio of melamine/TiO_2 is 4.5, the C+N-TiO_2/HNTs exhibited the best photocatalytic degradation efficiency of methyl blue (MB) under solar light irradiation. The obtained C+N-TiO_2/HNTs were characterized by transmission electron microscopy (TEM), N_2 adsorption-desorption isotherm (BET), X-ray photoelectron spectroscopy (XPS), and Fourier transform infrared spectrum (FT-IR). The results showed that the aggregation was effectively reduced, and TiO_2 nanoparticles could be uniformly deposited on the surface of HNTs. This leads to an increase of their specific surface area. XPS and FT-IR analyses indicated TiO_2 particles were doped successfully with C and N via the linkage of the Ti–O–N, O–Ti–N, and Ti–O–C. Photocatalytic experiments showed that C+N-TiO_2/HNTs had higher degradation efficiency of MB than TiO_2/HNTs. This makes the composite a potential candidate for the photocatalytic wastewater treatment.

1. Introduction

Industrial dyes are one of the main sources of water contamination, which are enormously harmful to ecological environment and human beings [1, 2]. Numerous representative methods, including Fenton oxidation, biological treatment, photocatalytic degradation, membrane filtration, and adsorption [3–7], have been employed to remove the organic dyes from polluted wastewater. Photocatalysis has been commonly deemed to be a mature and reliable technique for the wastewater treatment. In the past decades, enormous efforts have been devoted to researching oxide semiconductor photocatalysts with high activities for environmental protection [8–10]. As a promising solar-driven photocatalyst, anatase titania (TiO_2) has attracted tremendous attentions for water cleaning. However, some malpractices of anatase TiO_2 are still under concern: (a) the agglomerates, composed of the primary small particles, increase the size of TiO_2; (b) the ability of visible-light response is not satisfactory. Therefore, much effort has been made on anatase to improve its visible-light photocatalytic capability by controlling its microstructure (morphology, size, crystallinity, and facets) and by tuning its band structure near the valence maximum and conduction band minimum (with element doping, oxygen vacancies, etc.) [11, 12]. Among them, element doping impurities may be alternative for the extension of photocatalytic activity of TiO_2 into the visible region compared to other methods because the doping element states are near the valence band edge. The several nonmetal codoped TiO_2 materials, such as nitrogen/fluorine [9], sulfur/nitrogen [13], and carbon/nitrogen [14, 15], mainly based on nitrogen doping effect, could result in higher visible-light responses as compared to the TiO_2 doped with single element.

As a sort of available aluminosilicate clay, halloysite nanotubes (HNTs) have been intensively investigated in the treatment of dye wastewater [16–18] due to their well-defined hollow tubular structure with ca.15 nm diameter lumen and 600–1500 nm length averagely [19], which owns a large specific surface area and more complicated pore distribution. Furthermore, the clay nanotubes possess the advantages of large surface area, high porosity, and tunable surface chemistry, which enable this nanomaterial to be utilized as an attractive support for the assembly of small metal and metal oxide. Thus, depositing the TiO_2 nanoparticles onto HNTs is a promising method to block their aggregation. Then HNTs can be directly used to support the TiO_2 nanoparticles because of these hydroxyl groups. The combination of TiO_2 and HNTs is promising to simultaneously possess excellent photocatalytic activity and absorptivity, which could deliver exceptional performances in photocatalytic degradation of organics.

In this work, TiO_2/amorphous halloysite composites were facilely fabricated by a "precipitation-dissolution-recrystallization" route at a low temperature, and then C+N codoped TiO_2/amorphous halloysite photocatalysts were obtained using melamine as C+N source at a high temperature. The performance of TiO_2/amorphous halloysite composites incorporating C+N codoped TiO_2/amorphous halloysite photocatalysts on the photocatalytic degradation of methyl blue (MB) under solar light is studied.

2. Experimental

2.1. Preparation of C+N Codoped TiO_2/Amorphous Halloysite Composite Catalysts (C+N-TiO_2/HNTs). TiO_2/amorphous halloysite composites were fabricated by a "precipitation-dissolution-recrystallization" route. The concrete procedures were as follows: titanium tetrachloride ($TiCl_4$) solution (2.3 M, 60 mL) was put into the flask with four necks, and then NaOH solution (2.5 M, 165 mL) was added dropwise into the above $TiCl_4$ solution with vigorous agitation. The reaction temperature was controlled and set to 10°C. The turbid solution was obtained at the end of reaction. Subsequently, the system temperature was controlled to 80°C, halloysite dispersion (0.068 g/mL, 320 mL) was added rapidly into the above solution when the turbid solution began to clarify, and finally the whole mixture was kept at 80°C for 4 h. The obtained TiO_2/amorphous halloysite dispersion was filtrated and washed with deionized water, and the as-prepared TiO_2/amorphous halloysite composites were again mixed with melamine (MA), and the obtained uniform slurry mixture was placed into a muffle furnace at 550°C for 4 h. With this, the yellow powders C+N-TiO_2/HNTs were completely formed. For comparison, C+N-TiO_2 and TiO_2/HNTs catalysts were prepared under similar conditions.

2.2. Characterizations. X-ray diffraction (XRD) patterns were recorded on D/Max 2500 PC X-ray diffractometer (Rigaku Corporation, Japan) with Cu Kα radiation of the X-ray wavelength 0.15418 nm over a 2θ range (5~80°). The N_2 adsorption-desorption isotherms and pore distribution (Brunauer-Emmett-Teller, BET, method) were determined by Micromeritics Corporation ASAP2010C surface area and porosimetry system. The morphologies of the as-obtained samples were observed by JEOL Corporation (Japan) JEM-2100 transmission electron microscopy (TEM). X-ray photoelectron spectroscopy (XPS) measurement was carried out by VG Corporation (UK) ESCALAB MKII with an Al Kα X-ray source. Fourier transform infrared (FT-IR) spectrum was performed by a Nicolet Avatar 370 (Thermo Corporation, USA) from 4000 to 400 cm^{-1}. The UV-vis absorption spectra were measured under the diffused reflection mode using the integrating sphere (UV2401/2, Shimadu, Japan) attached to a Shimadu 2550 UV-vis spectrometer.

2.3. Evaluation of Photocatalytic Activity. The photocatalytic activities of the obtained photocatalysts were tested by the degradation of methylene blue (MB) under simulated solar light irradiation in the vessel with Xeon lamp (300 W). 0.03 g of catalyst powders were dispersed in aqueous solution of MB (500 mL, 20 mg/L) by ultrasonication and oscillation, and the obtained mixture was sonicated. Prior to irradiation, the dispersions were magnetically stirred in dark for 30 min. During the MB photodecomposition, samples were withdrawn at regular intervals (10 min) and centrifuged to separate solid particles for analysis. The concentration of aqueous MB was determined using 722 vis spectrophotometer by measuring its absorbance at the range of 664 nm. The MB degradation was calculated by Lambert-Beer equation (1), where A_0 is the initial absorbance of the MB solution ($A_0 = 1.525$), A_t is the absorbance of MB solution after irradiation, and η is photodegradation yield. Photoactivities for MB in the dark in the presence of the photocatalyst and under solar light irradiation in the absence of the photocatalyst were also evaluated as follows:

$$\eta = \frac{A_0 - A_t}{A_0} \times 100\%. \quad (1)$$

3. Results and Discussion

3.1. XRD Analysis. To ascertain the structures of the products, XRD patterns of HNTs and TiO_2/HNTs with different mass ratios of MA and TiO_2 are shown in Figure 1. The XRD reflections of HNTs at $2\theta = 12.1°, 19.9°$, and 24.8° in accordance with reflection planes (001), (020), (110), and (002) [20] disappear after calcination, suggesting that the crystal structure of HNTs has been destroyed. The result is in agreement with the previous report [21]. However, the tube-like morphology of HNTs can be still maintained from the following TEM in Figure 3. Besides, it can be seen that calcined TiO_2/HNTs and C+N-TiO_2/HNTs of different ratios exhibit anatase crystal at $2\theta = 25.2°, 38.2°, 47.8°, 54.5°$, and 62.6° in accordance with reflection planes (101), (004), (200), (105), and (204), which indicates that anatase TiO_2 is fabricated successfully and the TiO_2 crystal phase has no appreciable changes by C+N doping.

3.2. UV-vis Analysis. The optical properties of TiO_2/HNTs and C+N-TiO_2/HNTs are examined by UV-vis absorption spectra in Figure 2. Obviously, the absorption edges of C+N codoped TiO_2/HNTs shift to the visible range in comparison

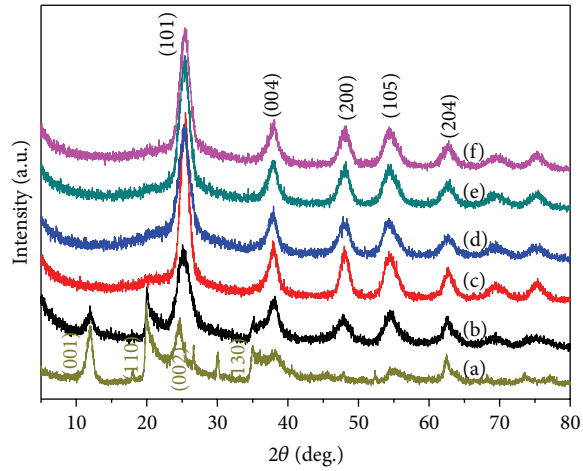

Figure 1: XRD patterns of pure HNTs, TiO_2/HNTs, and C+N-HNTs/TiO_2 at various ratios (m(MA) : m(TiO_2)). (a) Pure HNTs, (b) TiO_2/HNTs, (c) calcined TiO_2/HNTs, (d) C+N-HNTs/TiO_2 (4.5 : 1), (e) C+N-HNTs/TiO_2 (2.2 : 1), and (f) C+N-HNTs/TiO_2 (3.3 : 1).

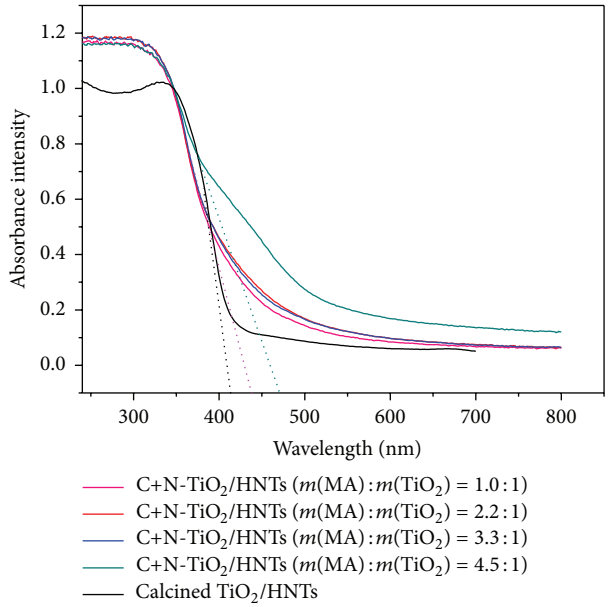

Figure 2: UV-vis diffuse reflectance spectra of HNTs/TiO_2 and C+N-HNTs/TiO_2 at various ratios.

with those of original TiO_2/HNTs, indicating that the doping of C and N modifies the bandgap energy of TiO_2. In addition, the red shift of C+N-TiO_2/HNTs is slightly different with the increasing dosage of MA, demonstrating that the MA dosage shows important impact on the properties of TiO_2. In addition, the samples of C+N-TiO_2/HNTs show the highest red shift when the mass ratio of MA and TiO_2 is 4.5, in which the wavelength is extended to approximately 470 nm, further shifting to the visible region. This result is in accordance with the theoretical electronic structure calculation that the C+N codoped TiO_2 presents strong visible-light absorption in the range of 400–600 nm [22]. The observation implies that C+N-TiO_2/HNTs (mass ratio of MA and TiO_2 is 4.5, C+N-TiO_2/HNTs (4.5)) may have preferable photocatalytic performance.

3.3. TEM Analysis. The morphologies of HNTs, TiO_2, TiO_2/HNTs, and C+N-TiO_2/HNTs (4.5) are analyzed by TEM as shown in Figure 3. Pristine halloysite is a cylindrical-shaped tube with multilayer walls. Generally, the HNTs contain agglomerates of nanotubes with some irregularities in diameter, wall thickness, and morphology [23] (Figure 3(a)). Serious aggregation of the oblate-like C+N-TiO_2 particles obtained under similar conditions can be found (Figure 3(b)), and the length of particles is ~100 nm and the width is ~30 nm. However, TiO_2 particles are uniformly deposited on the surface of HNTs, indicating that aggregation is effectively prevented by introducing HNTs (Figure 3(c)). Comparing the TEM image of C+N-TiO_2 (Figure 3(b)) with those of C+N-TiO_2/HNTs (Figure 3(d)), TiO_2 nanoparticles are uniformly dispersed without apparent aggregation on the surface of

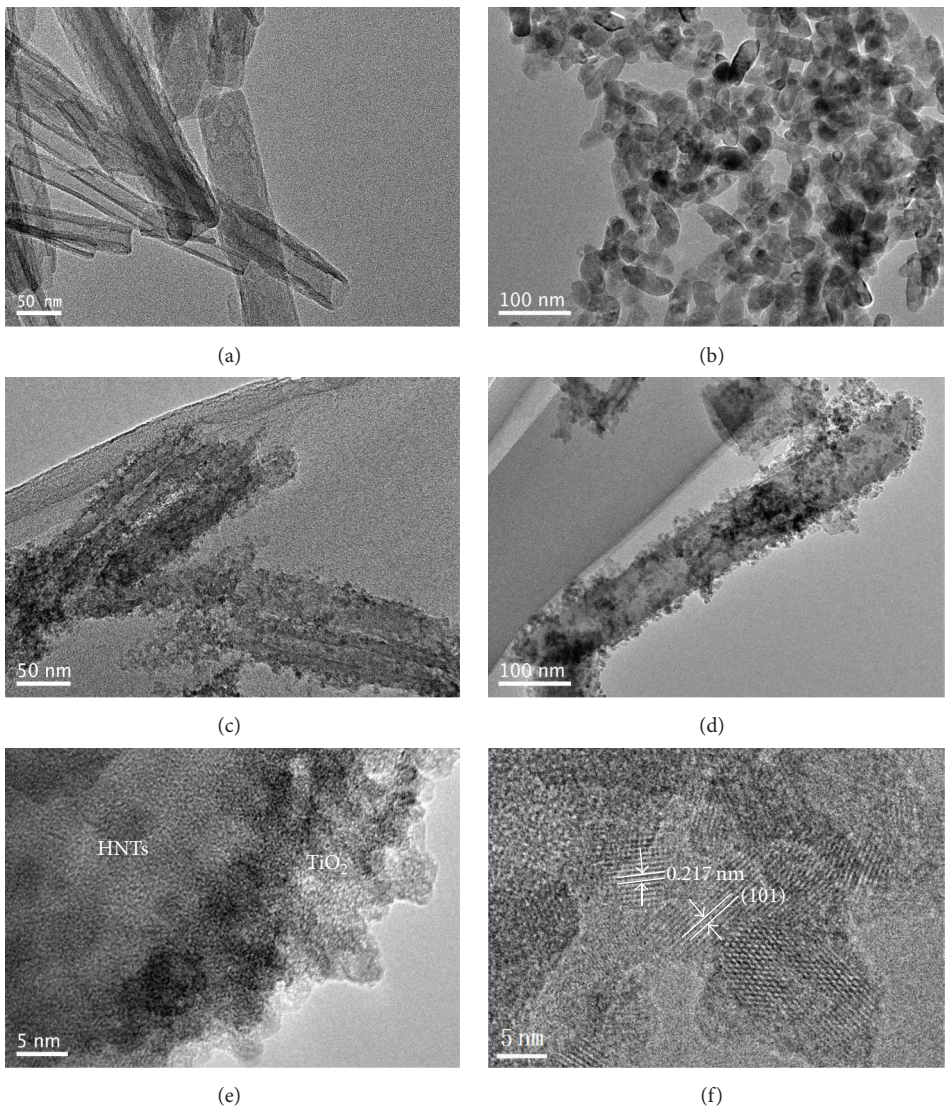

Figure 3: TEM micrographs: (a) HNTs, (b) TiO_2, (c) TiO_2/HNTs, (d) C+N-TiO_2/HNTs, (e) HRTEM of C+N-TiO_2/HNTs, and (f) magnified TEM image of (e).

HNTs. In addition, the size of C+N-TiO_2 on the HNTs surface (Figure 3(d)) enormously decreases in comparison with that of the pure C+N-TiO_2 (Figure 3(b)), which demonstrates that the agglomeration and the size of C+N-TiO_2 could be controlled effectively. To further obtain the structural information, the C+N-TiO_2/HNTs are characterized by HRTEM (Figures 3(e) and 3(f)). As can be seen, the particle size of C+N-TiO_2 on the HNTs surface is 5~10 nm, and the interplanar spacing of 0.217 nm corresponds to the (101) planes of anatase TiO_2 phase.

3.4. Determination of Specific Surface Area and Porosity. The N_2 adsorption-desorption isotherms and pore size distributions for three materials are presented in Figure 4. The isotherm shapes for the composites are similar (Type IV, IUPAC classification), which are indicative of the presence of mesopores. The adsorbed N_2 volume of calcined TiO_2/HNTs, as well as C+N-TiO_2/HNTs, is larger than that of HNTs (Figure 4(a)), and the total pore volume and the pore size (6~8 nm) of these composites are found to be significantly higher than HNTs (Figure 4(b)). The BET specific surface areas are measured to be 174.28 m^2/g, 123.13 m^2/g, and 42.92 m^2/g for C+N-TiO_2/HNTs, TiO_2/HNTs, and HNTs, respectively. The phenomena could be attributed to the presence of more interparticle pores of the composites and a better TiO_2 distribution on HNTs [24], which may be beneficial to dark adsorption for dye. The above results are in good agreement with those of TEM.

3.5. XPS and FT-IR Analysis. Chemical states of incorporated dopants in the as-prepared materials are determined by XPS (Figure 5). The binding energy (BE) distribution of Ti 2p for calcined TiO_2/HNTs shifts to high binding energy direction compared with that of pristine TiO_2, suggesting the

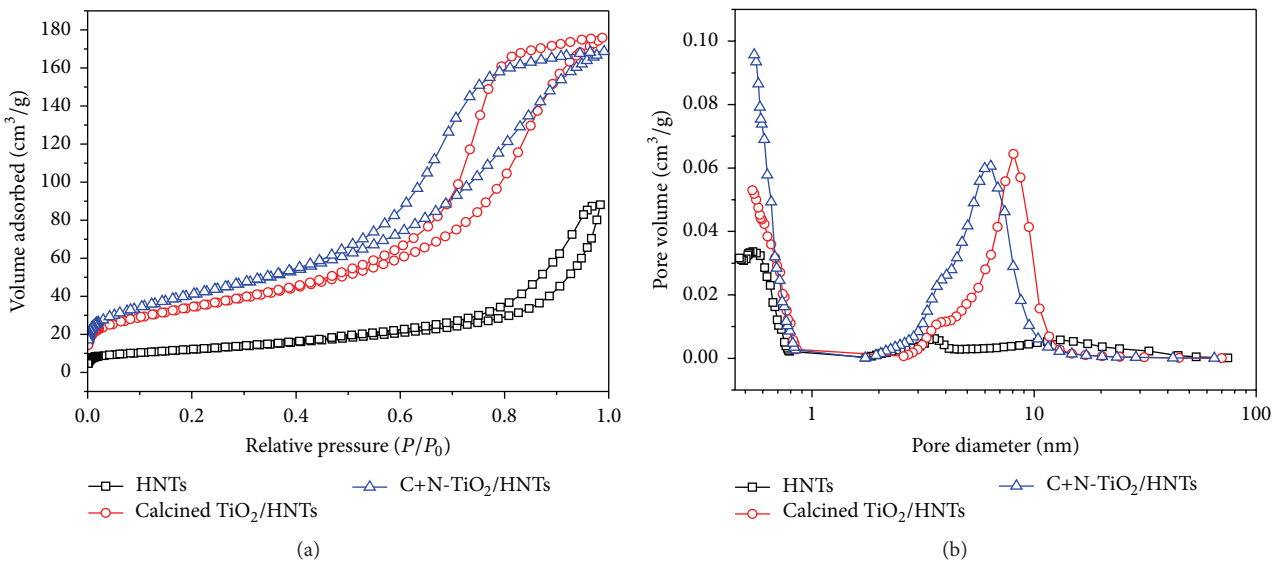

FIGURE 4: N_2 adsorption-desorption isotherms (a) and pore distribution (b) of HNTs, TiO_2/HNTs, and C+N-TiO_2/HNTs.

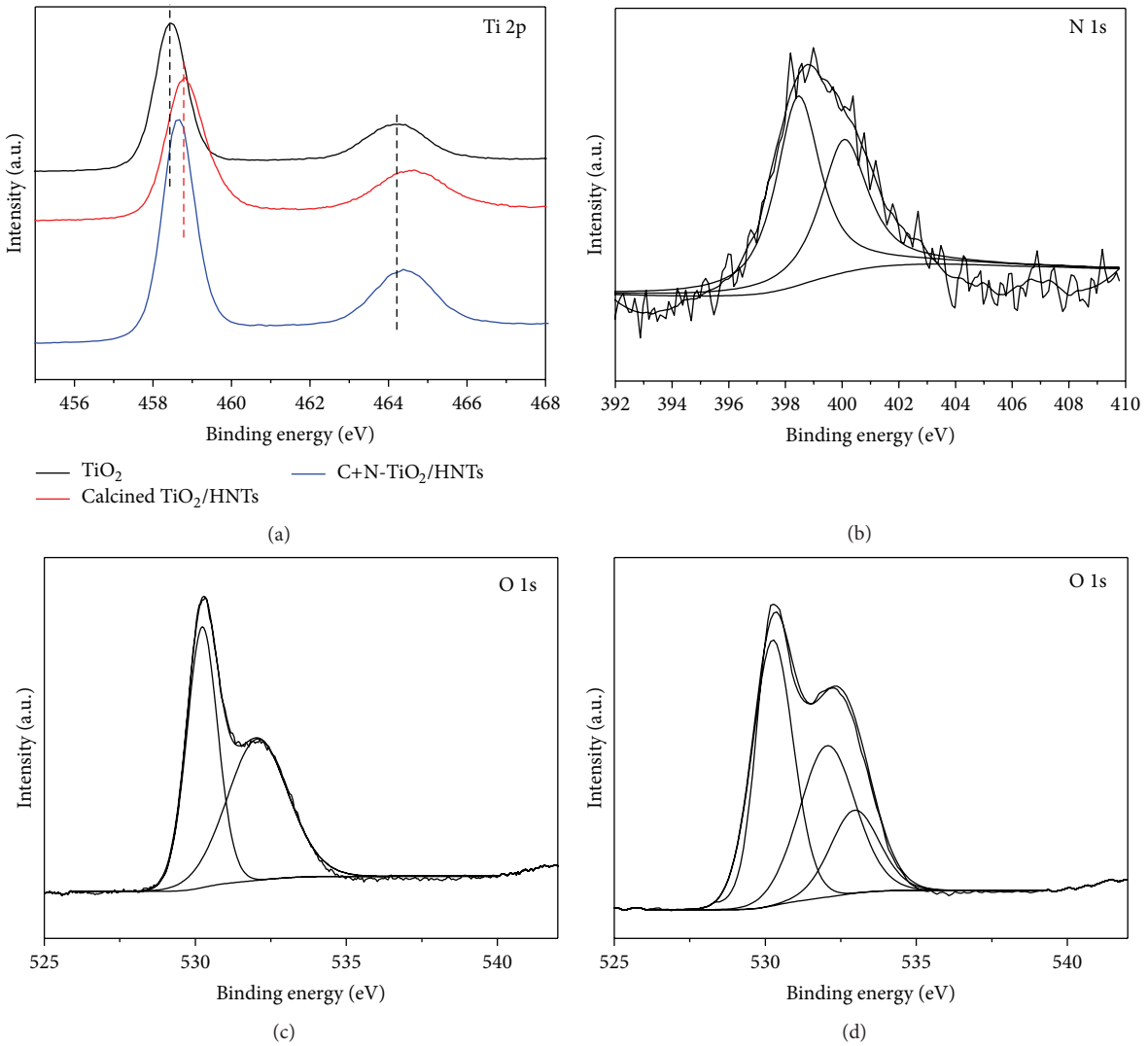

FIGURE 5: XPS analysis of (a) Ti 2p spectra of all the samples reoffered here; (b) N 1s and (c) O 1s spectra of calcined TiO_2/HNTs; (d) O 1s of C+N-TiO_2/HNTs.

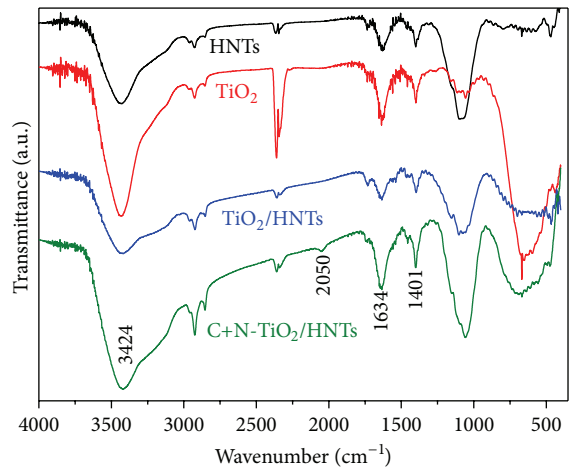

Figure 6: FT-IR spectra of HNTs, TiO_2, calcined TiO_2/HNTs, and C+N-TiO_2/HNTs.

formation of Ti–O–Si bond (Figure 5(a)). The electronegativity of Ti is less than that of Si, which makes the BE of Ti 2p of Ti–O–Ti be lower than that of Ti–O–Si. For C+N-TiO_2/HNTs, the lattice incorporation of N generates Ti–N bonds by the partial replacement of O^{2-} with N^- (Figure 5(a)). This gives rise to an increase in the electron density on Ti due to the fact that the electronegativity of the N atom is smaller than the O atom and partial reduction of Ti^{4+} to Ti^{3+} occurs, which manifests as a slightly decrease in Ti 2p binding energy [25]. The core level of N 1s for C+N-TiO_2/HNTs can be fitted into two peaks at 398.5 eV and 400.1 eV, respectively (Figure 5(b)). The first major peak at 398.5 eV is assigned to the substituted N in the form of O–Ti–N [26, 27], indicating that partial of O atoms in the lattice of TiO_2 is substituted by N^- anions. The analysis is in agreement with that of Ti 2p result. The latter minor peak is attributed to the interstitial N-doping or the formation of Ti–O–N species [28]. Furthermore, XPS spectra of O 1s for calcined TiO_2/HNTs and C+N-TiO_2/HNTs are analyzed. The O 1s peak of calcined TiO_2/HNTs (Figure 5(c)) can be fitted into two components centered at 530.1 eV and 532.0 eV. The first component is attributed to lattice oxygen in TiO_2, while the second one can be assigned to oxygen atoms of Si–O/Al–O bonds. For C+N-TiO_2/HNTs, the O 1s spectra can be fitted into three components. The first two components at 530.0 eV and 532.2 eV are similar to those of calcined TiO_2/HNTs. The newly emerged component is centered at 532.8 eV; it may be ascribed to O 1s originated from Ti–O–C (Ti–O=C) or Ti–O–N groups due to the substitution of carbon for some of the lattice titanium atom [12]. These findings agree well with the results of UV-vis analyses, which are responsible for the high photocatalytic activity.

In order to provide additional evidence of the codoping C and N, FT-IR spectra are performed (Figure 6). The broadband at 3424 cm^{-1} could be ascribed to the stretch vibration of O–H, whereas the peaks at 1634 cm^{-1} and 1401 cm^{-1} could be assigned to the bending vibrations of O–H formed by adsorbed water molecules and N–H groups [29]. It has been reported that codoping with C and N increased the amount of surface adsorbed water and hydroxyl groups [30]. Clearly, the intensity of hydroxyl groups from C+N-TiO_2/HNTs noticeably increases compared to that of the pure TiO_2/HNTs, and a new peak at 2050 cm^{-1} from C+N-TiO_2/HNTs can be observed, which indicated that TiO_2 may be codoped with C and N after calcination.

3.6. Photocatalytic Activity. The photodegradation of MB by calcined TiO_2/HNTs and C+N-TiO_2/HNTs are presented in Figure 7. Apparently, calcined TiO_2/HNTs and C+N-TiO_2/HNTs show negligible ability to absorb MB in the dark (Figure 7(a), inset). The two catalysts exhibit satisfactory photodegradation of MB under solar light irradiation. When MB is exposed for 1 h, approximately 85% and 95% of MB are removed by TiO_2/HNTs and C+N-TiO_2/HNTs, respectively. However, C+N-TiO_2/HNTs display more excellent performance in comparison with TiO_2/HNTs (Figure 7(a)). The better adsorption and photodegradation of MB by C+N-TiO_2/HNTs are ascribed to the larger BET surface and the better doping of TiO_2. To evaluate its usefulness, the two catalysts are reused five times for photodegradation (Figure 7(b)). After five cycles, the degradation effectiveness decreases rapidly for TiO_2/HNTs, which indicates that photodegradation by C+N-TiO_2/HNTs remain steady and more effective than TiO_2/HNTs under successive solar light.

4. Conclusions

C and N codoped anatase TiO_2/HNT photocatalysts with a series of mass ratios of melamine and TiO_2 have been successfully synthesised. It is found that the photoactivity of C+N-TiO_2/HNTs can be clearly improved when the mass ratio of melamine and TiO_2 is 4.5. The anatase TiO_2 nanoparticles can be uniformly deposited on the surface of HNTs, and their particle size decreases compared with the analogous TiO_2. Consequently, the C+N-TiO_2/HNTs exhibit steadier and more effective adsorption and photodegradation

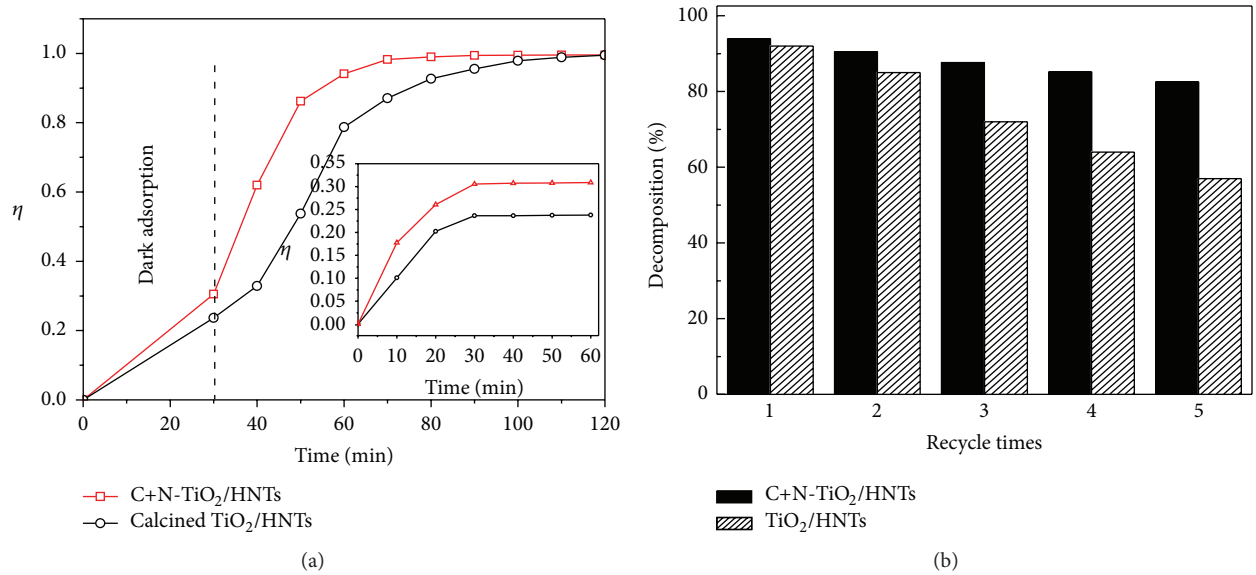

FIGURE 7: (a) Photocatalytic degradation and dark adsorption (inset) of calcined TiO_2/HNTs and C+N-TiO_2/HNTs; (b) stability of the photocatalysts after 5 cycles of photocatalytic decomposition of MB.

due to the larger BET surface and the better doping than TiO_2/HNTs. Experiments prove that C+N-TiO_2/HNTs can be employed repeatedly as a promising candidate for the treatment of dye wastewater.

Conflict of Interests

The authors declare that there is no conflict of interests regarding the publication of this paper.

Acknowledgments

The authors gratefully acknowledge funding for this work provided by the National Nature Sciences Foundation of China (Grant no. 21303118), Specialized Research Fund for the Doctoral Program of Higher Education (no. 2013-0032120003), and the Seed Foundation of Tianjin University.

References

[1] L. A. Vasil'eva, L. N. Pylev, M. Sikora, D. Guretska, and E. Gurska, "Mutagenicity and harmful effects of anthraquinone dyes on DNA," *Gigiena Truda i Professional'nye Zabolevaniia*, no. 5, pp. 28–30, 1989.

[2] I. M. Grushko and S. S. Timofeeva, "Dyes and their harmful action on the body," *Gigiena i Sanitariia*, vol. 8, no. 75, 1983.

[3] T.-H. Kim, C. Park, J. M. Yang, and S. Kim, "Comparison of disperse and reactive dye removals by chemical coagulation and Fenton oxidation," *Journal of Hazardous Materials*, vol. 112, no. 1-2, pp. 95–103, 2004.

[4] T.-H. Kim, C. Park, and S. Kim, "Water recycling from desalination and purification process of reactive dye manufacturing industry by combined membrane filtration," *Journal of Cleaner Production*, vol. 13, no. 8, pp. 779–786, 2005.

[5] M. M. Ayad and A. A. El-Nasr, "Adsorption of cationic dye (methylene blue) from water using polyaniline nanotubes base," *The Journal of Physical Chemistry C*, vol. 114, no. 34, pp. 14377–14383, 2010.

[6] O. Türgay, G. Ersöz, S. Atalay, J. Forss, and U. Welander, "The treatment of azo dyes found in textile industry wastewater by anaerobic biological method and chemical oxidation," *Separation and Purification Technology*, vol. 79, no. 1, pp. 26–33, 2011.

[7] L. Andronic and A. Duta, "Photodegradation processes in two-dyes systems—simultaneous analysis by first-order spectra derivative method," *Chemical Engineering Journal*, vol. 198-199, pp. 468–475, 2012.

[8] A. Mills and S. Le Hunte, "An overview of semiconductor photocatalysis," *Journal of Photochemistry and Photobiology A: Chemistry*, vol. 108, no. 1, pp. 1–35, 1997.

[9] M. Pelaez, A. A. de la Cruz, E. Stathatos, P. Falaras, and D. D. Dionysiou, "Visible light-activated N-F-codoped TiO_2 nanoparticles for the photocatalytic degradation of microcystin-LR in water," *Catalysis Today*, vol. 144, no. 1-2, pp. 19–25, 2009.

[10] S. M. Saqer, D. I. Kondarides, and X. E. Verykios, "Catalytic oxidation of toluene over binary mixtures of copper, manganese and cerium oxides supported on γ-Al_2O_3," *Applied Catalysis B: Environmental*, vol. 103, no. 3-4, pp. 275–286, 2011.

[11] C. Yang, Z. Wang, T. Lin et al., "Core-shell nanostructured 'black' rutile titania as excellent catalyst for hydrogen production enhanced by sulfur doping," *Journal of the American Chemical Society*, vol. 135, no. 47, pp. 17831–17838, 2013.

[12] H. L. Chen, K.-F. Chen, S.-W. Lai, Z. Dang, and Y.-P. Peng, "Photoelectrochemical oxidation of azo dye and generation of hydrogen via C–N co-doped TiO_2 nanotube arrays," *Separation and Purification Technology*, vol. 146, pp. 143–153, 2015.

[13] J. A. Rengifo-Herrera, K. Pierzchała, A. Sienkiewicz et al., "Synthesis, characterization, and photocatalytic activities of nanoparticulate N, S-codoped TiO_2 having different surface-to-volume ratios," *The Journal of Physical Chemistry C*, vol. 114, no. 6, pp. 2717–2723, 2010.

[14] J. Wang, B. Huang, Z. Wang, X. Qin, and X. Zhang, "Synthesis and characterization of C, N-codoped TiO_2 nanotubes/nanorods with visible-light activity," *Rare Metals*, vol. 30, no. 1, pp. 161–165, 2011.

[15] G. Dai, S. Liu, Y. Liang, H. Liu, and Z. Zhong, "A simple preparation of carbon and nitrogen co-doped nanoscaled TiO_2 with exposed {0 0 1} facets for enhanced visible-light photocatalytic activity," *Journal of Molecular Catalysis A: Chemical*, vol. 368-369, pp. 38–42, 2013.

[16] L. Liu, Y. Z. Wan, Y. D. Xie, R. Zhai, B. Zhang, and J. D. Liu, "The removal of dye from aqueous solution using alginate-halloysite nanotube beads," *Chemical Engineering Journal*, vol. 187, pp. 210–216, 2012.

[17] G. Kiani, M. Dostali, A. Rostami, and A. R. Khataee, "Adsorption studies on the removal of Malachite Green from aqueous solutions onto halloysite nanotubes," *Applied Clay Science*, vol. 54, no. 1, pp. 34–39, 2011.

[18] P. Luo, Y. F. Zhao, B. Zhang, J. D. Liu, Y. Yang, and J. F. Liu, "Study on the adsorption of Neutral Red from aqueous solution onto halloysite nanotubes," *Water Research*, vol. 44, no. 5, pp. 1489–1497, 2010.

[19] E. Abdullayev, K. Sakakibara, K. Okamoto, W. Wei, K. Ariga, and Y. Lvov, "Natural tubule clay template synthesis of silver nanorods for antibacterial composite coating," *ACS Applied Materials and Interfaces*, vol. 3, no. 10, pp. 4040–4046, 2011.

[20] M. X. Liu, Y. Zhang, and C. R. Zhou, "Nanocomposites of halloysite and polylactide," *Applied Clay Science*, vol. 75-76, pp. 52–59, 2013.

[21] L. Jiang, Y. Huang, and T. Liu, "Enhanced visible-light photocatalytic performance of electrospun carbon-doped TiO_2/halloysite nanotube hybrid nanofibers," *Journal of Colloid and Interface Science*, vol. 439, pp. 62–68, 2015.

[22] M. Guo and J. Du, "Electronic and optical properties of C–N-codoped TiO_2: a first-principles GGA+U investigation N," *International Journal of Modern Physics B*, vol. 27, no. 23, Article ID 1350123, 2013.

[23] W. O. Yah, A. Takahara, and Y. M. Lvov, "Selective modification of halloysite lumen with octadecylphosphonic acid: new inorganic tubular micelle," *Journal of the American Chemical Society*, vol. 134, no. 3, pp. 1853–1859, 2012.

[24] D. Papoulis, S. Komarneni, D. Panagiotaras et al., "Halloysite-TiO_2 nanocomposites: synthesis, characterization and photocatalytic activity," *Applied Catalysis B: Environmental*, vol. 132-133, pp. 416–422, 2013.

[25] D.-H. Wang, L. Jia, X.-L. Wu, L.-Q. Lu, and A.-W. Xu, "One-step hydrothermal synthesis of N-doped TiO_2/C nanocomposites with high visible light photocatalytic activity," *Nanoscale*, vol. 4, no. 2, pp. 576–584, 2012.

[26] J.-H. Xu, J. X. Li, W.-L. Dai, Y. Cao, H. X. Li, and K. N. Fan, "Simple fabrication of twist-like helix N,S-codoped titania photocatalyst with visible-light response," *Applied Catalysis B: Environmental*, vol. 79, no. 1, pp. 72–80, 2008.

[27] H. Han and R. B. Bai, "Buoyant photocatalyst with greatly enhanced visible-light activity prepared through a low temperature hydrothermal method," *Industrial & Engineering Chemistry Research*, vol. 48, no. 6, pp. 2891–2898, 2009.

[28] X. W. Cheng, X. J. Yu, and Z. P. Xing, "Synthesis and characterization of C–N–S-tridoped TiO_2 nano-crystalline photocatalyst and its photocatalytic activity for degradation of rhodamine B," *Journal of Physics and Chemistry of Solids*, vol. 74, no. 5, pp. 684–690, 2013.

[29] W. Junwei, Z. Wei, Z. Yinqing, and L. Shuangxi, "An efficient two-step technique for nitrogen-doped titanium dioxide synthesizing: visible-light-induced photodecomposition of methylene blue," *Journal of Physical Chemistry C*, vol. 111, no. 2, pp. 1010–1014, 2007.

[30] X. W. Cheng, X. J. Yu, and Z. P. Xing, "Characterization and mechanism analysis of N doped TiO_2 with visible light response and its enhanced visible activity," *Applied Surface Science*, vol. 258, no. 7, pp. 3244–3248, 2012.

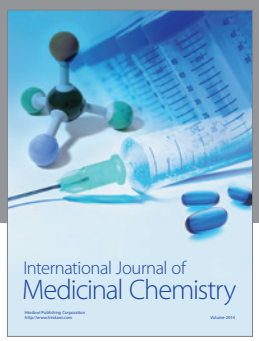

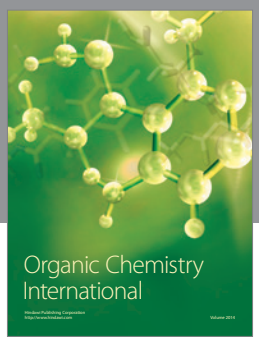

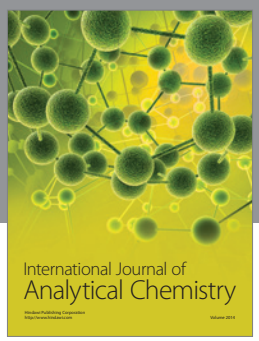

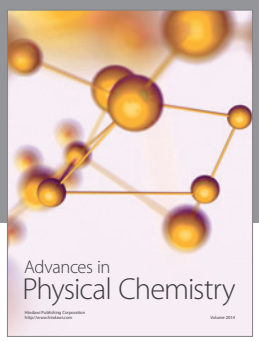

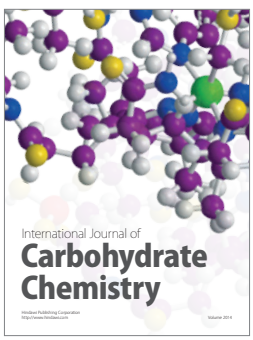

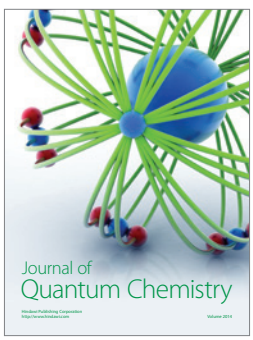

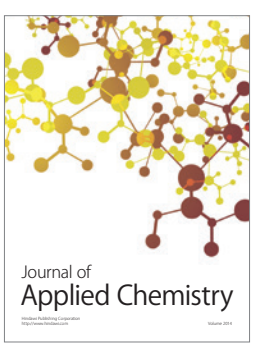

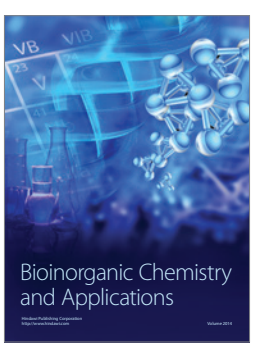

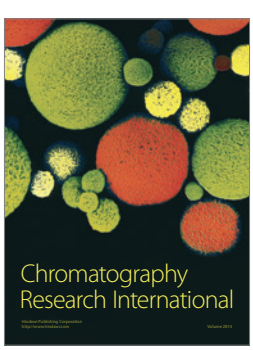

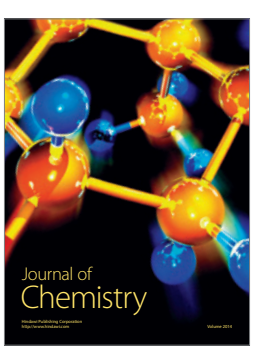

Hindawi

Submit your manuscripts at
http://www.hindawi.com